

# Throughput Optimization in UAV-Mounted RIS under Jittering and Imperfect CSI via DRL

Anas K. Saeed, Mahmoud M. Salim, Ali Arshad Nasir, *Senior Member, IEEE*,  
and Ali H. Muqaibel, *Senior Member, IEEE*

**Abstract**—Reconfigurable intelligent surfaces (RISs) mounted on unmanned aerial vehicles (UAVs) can reshape wireless propagation on-demand. However, their performance is sensitive to UAV jitter and cascaded channel uncertainty. This paper investigates a downlink multiple-input single-output UAV-mounted RIS system in which a ground multiple-antenna base station (BS) serves multiple single-antenna users under practical impairments. Our goal is to maximize the expected throughput under stochastic three-dimensional UAV jitter and imperfect cascaded channel state information (CSI) based only on the available channel estimates. This leads to a stochastic nonconvex optimization problem subject to a BS transmit power constraint and strict unit-modulus constraints on all RIS elements. To address this problem, we design a model-free deep reinforcement learning (DRL) framework with a contextual bandit formulation. A differentiable feasibility layer is utilized to map continuous actions to feasible solutions, while the reward is a Monte Carlo estimate of the expected throughput. We instantiate this framework with constrained variants of deep deterministic policy gradient (DDPG) and twin delayed deep deterministic policy gradient (TD3) that do not use target networks. Simulations show that the proposed algorithms yield higher throughput than conventional alternating optimization-based weighted minimum mean-square error (AO-WMMSE) baselines under severe jitter and low CSI quality. Across different scenarios, the proposed methods achieve performance that is either comparable to or slightly below the AO-WMMSE benchmark, based on sample average approximation (SAA) with a relative gap ranging from 0-12%. Moreover, the proposed DRL controllers achieve online inference times of 0.6 ms per decision versus roughly 370-550 ms for AO-WMMSE solvers.

**Index Terms**—CSI, DRL, jitter, RIS, UAV.

## I. INTRODUCTION

The demand for high connectivity continues to grow, driven by massive internet of things (IoT) connectivity. Wireless traffic is expected to increase dramatically toward 2030, posing significant challenges to the spectral and energy efficiency of existing fifth generation (5G) networks [1]. This growth requires ultra-reliable low-latency communications, higher density, and more adaptive systems.

All authors are with the Center for Communication Systems and Sensing, King Fahd University of Petroleum and Minerals, Dhahran 31261, Saudi Arabia. Also, Anas K. Saeed, Ali Arshad Nasir, and Ali H. Muqaibel are with the Electrical Engineering Department at King Fahd University of Petroleum and Minerals, Dhahran 31261, Saudi Arabia. Ali H. Muqaibel is the corresponding author (email: muqaibel@kfupm.edu.sa).

Sixth generation (6G) systems address current limitations [2].

Among the 6G enablers, reconfigurable intelligent surface (RIS) stands out as a low-power way to shape radio propagation [3]. An RIS is a thin surface with many passive elements [4]. By adjusting these elements, it can steer, reflect, or focus signals to improve coverage, reduce interference, and support beamforming. In parallel, unmanned aerial vehicles (UAVs) offer fast and flexible 3D placement. They can be deployed to restore line-of-sight (LoS) paths, bypass temporary blockages, and provide on-demand connectivity for IoT deployments [5]. Mounting an RIS on a UAV enables programmable control of the radio environment to extend coverage and improve throughput.

Realizing these benefits in practice requires careful treatment of two sources of uncertainty that the literature often simplifies. The first is UAV jitter caused by wind and control errors, which alters the effective array geometry and degrades beam alignment [6]. Another source of uncertainty is imperfect channel state information (CSI). Designs optimized under the assumption of perfect channel knowledge can suffer significant performance loss when the available channel estimates are outdated or corrupted by noise. Large numbers of low-cost IoT nodes and limited overhead make frequent high-quality CSI acquisition difficult [7]. In addition, RIS elements are passive and do not take part in pilot processing, which further complicates estimation.

Classical model-based designs are effective when channel models and CSI are accurate. However, UAV attitude variations and cascaded CSI uncertainty increase sensitivity to mismatch and reduce scalability [8]. Because the joint design is nonconvex, common methods such as alternating optimization (AO) and semidefinite relaxation (SDR) are only guaranteed to converge to stationary points, which can be suboptimal and often require many iterations [9]. Heuristic searches can reduce modeling effort but often trade solution quality and robustness for speed [10]. These limitations motivate a data-driven controller that can adapt online under partial models. We therefore adopt deep reinforcement learning (DRL) algorithms such as deep deterministic policy gradient (DDPG) and twin delayed deep deterministic policy gradient (TD3) for joint beamforming and RIS phase design.

## II. RELATED WORK

The integration of learning-based optimization into wireless networks has evolved rapidly, moving from static

terrestrial setups to mobility-aware aerial networks. First, we discuss foundational DRL approaches for static RIS deployments. Second, we examine the transition to UAV-mounted RIS architectures where mobility is a primary variable. Finally, we analyze existing robust designs, highlighting the gap in handling UAV jitter and imperfect CSI.

#### A. Static RIS Optimization via DRL

Early work applied DRL to jointly optimize beamforming and RIS phases. The authors in [11] pioneered the use of DRL in this domain and showed that actor-critic algorithms like DDPG could effectively maximize sum-rate (aggregate throughput) in continuous action spaces. However, a critical evolution in this literature questions the necessity of full Markov decision process (MDP) formulations for wireless channels. Recognizing that channel realizations in block-fading models are often independent and identically distributed (i.i.d.), recent studies have advocated for simplifying the problem to a contextual bandit formulation. For instance, the study in [12] demonstrated that a bandit-based approach could give comparable DRL performance with significantly lower computational overhead by discarding the temporal dependency of states. Similarly, the work in [13] proposed a deep contextual bandit DDPG framework, arguing that the bandit approach is more consistent with the i.i.d. channel model and offers sample-efficient alignment with the physical system.

#### B. UAV-Mounted RIS Networks

To overcome the blockage limitations of terrestrial deployments, recent research has shifted toward integrating RISs with UAVs. To address this complexity, recent works have adopted DRL to handle the high-dimensional state space more efficiently. For instance, the study in [14] formulated the capacity maximization problem as an MDP. They employed a double deep Q-network (DDQN) to jointly optimize the UAV heading and RIS phase shifts. The authors in [15] proposed an RIS-equipped UAV rate-splitting multiple access (RSMA) framework where successive convex approximation (SCA)/SDR and a DDPG agent jointly optimize UAV position, RIS phase shifts, and power allocation to maximize the sum secrecy rate. The authors in [16] investigated a UAV-mounted RIS simultaneous wireless information and power transfer (SWIPT) system. They adopted a TD3-based DRL framework to jointly optimize the time-space-splitting factor, base station (BS) transmit power, and RIS coefficients so as to maximize energy harvesting (EH) efficiency. Despite their algorithmic differences, these studies assumed stable UAV and ideal or perfectly known CSI.

#### C. Robustness to Imperfect CSI and UAV Jitter

While the integration of UAV and RIS is promising, ensuring robustness against environmental uncertainties remains challenging. In terrestrial settings, the authors in [17] studied robust secure transmission with imperfect

cascaded CSI, jointly optimizing transmit beamforming and RIS phases via AO with SDR. The authors in [19] considered an RIS-aided downlink and maximized the throughput using a soft actor-critic (SAC) policy under hardware impairments and imperfect CSI. However, the scenario is terrestrial and does not model UAV jitter. The authors in [18] optimized EH efficiency in a UAV-mounted RIS setting with three-dimensional rotational jitter using a smoothed softmax dual deep deterministic policy gradient (SD3) DRL controller while imperfect CSI is not explicitly modeled. Collectively, these efforts treated a single impairment class, either CSI/hardware mismatch [17], [19], [21] or UAV jitter [18].

A closely related work considered mobility and impairments, but under different modeling choices. The authors in [20] studied a downlink system where the UAV acts as an aerial BS and the RIS is fixed in space. They minimized transmit power by jointly optimizing the UAV trajectory, active beamforming, and RIS phases. Their robustness model relies on bounded angular perturbations for the UAV links and includes hardware impairments through a RIS phase noise model. These assumptions do not represent a UAV-mounted RIS, where three-dimensional rotational motion perturbs the RIS array geometry and directly impacts the cascaded channel. In addition, their uncertainty treatment does not model imperfect cascaded CSI as channel estimation uncertainty, since the phase-noise term captures hardware coefficient errors rather than cascaded-CSI quality. They further use a hybrid semi-unfolding deep neural network (HSUDNN) surrogate trained on outputs of an AO/semidefinite programming (SDP)-based optimizer, which requires solver-generated supervision and differs from our model-free policy learning.

#### D. Challenges and Motivation

Table I summarizes recent RIS-assisted works and contrasts their problem settings and solution approaches. In the table, CB denotes contextual bandit, Jitter indicates whether UAV platform instability is explicitly modeled, and Imperfect CSI refers to channel estimation uncertainty. Most prior studies focus on static RIS deployments or idealized aerial links that assume perfect stability and channel knowledge, or they treat jitter and channel uncertainty separately. This leaves the combined impact of three-dimensional rotational jitter and imperfect cascaded CSI largely unaddressed in UAV-mounted RIS downlinks. Moreover, many baselines rely on iterative optimization such as AO, which can incur high per-decision latency and limits rapid reconfiguration. This is particularly restrictive in dense IoT deployments, where pilot overhead and edge compute are limited and the controller must update quickly under time-varying links.

Motivated by the above, we present a practical multiple-input single-output (MISO) system where a ground BS communicates with multiple users via a jitter-prone UAV-mounted RIS. We use a model-free DRL

Table I  
COMPARISON OF RIS-RELATED WORKS

| Paper    | Scenario               | Metric           | Variables                           | Algorithm              | Formulation | Imperfect CSI                | Jitter          |
|----------|------------------------|------------------|-------------------------------------|------------------------|-------------|------------------------------|-----------------|
| [11]     | RIS                    | Sum-rate         | Beamformer + RIS                    | DDPG                   | MDP         | $\times$                     | $\times$        |
| [12]     | Multi-RIS              | Sum-rate         | Beamformer + RIS                    | Deep Contextual Bandit | CB          | $\times$                     | $\times$        |
| [13]     | RIS                    | Sum-rate         | Beamformer + RIS                    | DDPG                   | CB          | $\times$                     | $\times$        |
| [14]     | UAV + RIS              | Capacity         | UAV traj. + RIS                     | DDQN                   | MDP         | $\times$                     | $\times$        |
| [15]     | UAV + RIS (RSMA)       | Sum secrecy rate | Beamformer + RIS + UAV traj.        | SCA + SDR + DDPG + AO  | MDP         | $\times$                     | $\times$        |
| [16]     | UAV + RIS              | EH efficiency    | TS factor $\tau$ + Power + RIS      | TD3                    | MDP         | $\times$                     | $\times$        |
| [17]     | RIS                    | Secrecy / power  | Beamformer + RIS                    | AO + SDR               | —           | Statistical error            | $\times$        |
| [18]     | UAV + RIS              | EH efficiency    | TS factor $\tau$ + Beamformer + RIS | SD3                    | MDP         | $\times$                     | Rotational-3D   |
| [19]     | RIS                    | Sum-rate         | Beamformer + RIS                    | SAC                    | MDP         | Statistical error            | $\times$        |
| [20]     | UAV (BS) + RIS (fixed) | Power            | Beamformer + RIS + UAV traj.        | AO + SDP + HSUDNN      | —           | $\times$                     | Bounded angular |
| Proposed | UAV + RIS              | Throughput       | Beamformer + RIS                    | DDPG + TD3             | CB          | Correlated statistical error | Rotational-3D   |

framework cast as a contextual bandit for optimization. We consider practical constraints such as 3D rotational jitter, channel estimation errors, a BS transmit power constraint, and strict unit-modulus constraints on the RIS elements, providing a more resilient and scalable UAV-RIS architecture. Specifically, the main contributions of this paper can be summarized as follows:

- A unified uncertainty model that captures UAV jitter and imperfect cascaded CSI is developed. This aligns the design with practical deployment impairments in UAV-mounted RIS links.
- A constrained contextual bandit based DRL framework is proposed for robust joint BS beamforming and RIS phase control under the developed uncertainty model. The proposed framework is instantiated with DDPG and TD3 backbones.
- A Monte Carlo reward is introduced to estimate the expected throughput by resampling jitter and CSI error realizations at each decision step. A differentiable safety layer is introduced to project unconstrained policy outputs to satisfy the BS transmit power constraint and the unit-modulus constraints on the RIS elements.
- Comprehensive evaluation is conducted against AO and weighted minimum mean-square error (WMMSE)-based baselines, including a robust sample average approximation (SAA) variant and beamformer-only ablations. The results are complemented by a complexity analysis demonstrating sub-millisecond online inference and lower computational complexity than the baselines.

### III. SYSTEM MODEL AND PROBLEM FORMULATION

#### A. System Architecture

We consider a downlink multiuser MISO communication system. We assume that the direct communication links between a ground-based BS and multiple ground users are nonexistent due to severe blockages. To overcome this, a UAV-mounted RIS is employed to create a reflective communications path. The system, as illustrated in Fig. 1, is modeled within a 3D Cartesian coordinate system.

The system's transmitter is a ground-based BS, located at a fixed position  $\mathbf{p}_{BS} \in \mathbb{R}^3$ . It is equipped with

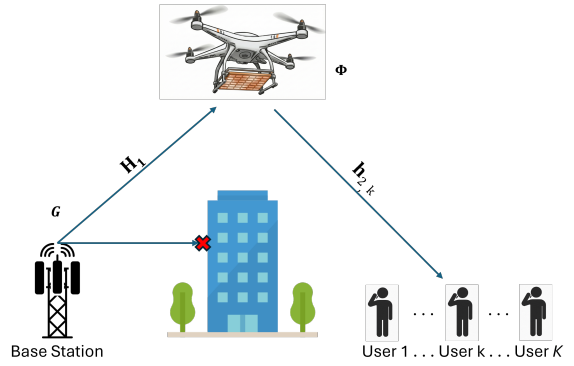


Fig. 1. UAV-mounted RIS communication system model

a uniform linear array (ULA) of  $M$  antennas oriented along the  $z$ -axis, with an inter-element spacing of  $\lambda_c/2$ , and operates under a maximum transmit power constraint,  $P_{\max}$ . Furthermore, the system serves  $K$  single-antenna ground users. The locations of these  $K$  users, denoted by  $\{\mathbf{p}_k \in \mathbb{R}^3\}_{k=1}^K$ , are randomly selected from a larger, predefined set of possible locations to increase generality. The communications model relies exclusively on the two-hop BS-RIS-user link. We consider a UAV deployed at a fixed, static location  $\mathbf{q}_{UAV} \in \mathbb{R}^3$ . The UAV carries an RIS with  $N$  passive reflecting elements arranged in a uniform planar array (UPA) on the  $xy$ -plane, with an inter-element spacing of  $\lambda_c/2$ . Each element can apply an independent phase shift to the incident signal.

#### B. Communications Model

Communication from the BS to the  $K$  users is facilitated by the cascaded BS-RIS-user link. The BS employs a linear precoding matrix  $\mathbf{G} \in \mathbb{C}^{M \times K}$  to encode the data symbol vector  $\mathbf{x} = [x_1, \dots, x_K]^T \in \mathbb{C}^{K \times 1}$ . We write  $\mathbf{G} = [\mathbf{g}_1, \dots, \mathbf{g}_K]$  with  $\mathbf{g}_k \in \mathbb{C}^{M \times 1}$ . Also, we assume the transmitted symbols are uncorrelated, each with unit power per stream, i.e.,  $\mathbb{E}[\mathbf{x}\mathbf{x}^H] = \mathbf{I}_K$ . The signal received at the  $k$ -th user is then given by

$$y_k = \mathbf{h}_{2,k}^H \Phi \mathbf{H}_1 \mathbf{G} \mathbf{x} + n_k, \quad (1)$$

where  $\mathbf{H}_1 \in \mathbb{C}^{N \times M}$  is the channel matrix for the first hop (BS-RIS),  $\mathbf{h}_{2,k} \in \mathbb{C}^{N \times 1}$  is the channel vector for the second hop (RIS-user  $k$ ),  $n_k \sim \mathcal{CN}(0, \sigma_n^2)$  is the additive white

Gaussian noise, and  $\Phi = \text{diag}(e^{j\theta_1}, \dots, e^{j\theta_N}) \in \mathbb{C}^{N \times N}$  represents the phase shifts applied by the RIS. The first hop channel,  $\mathbf{H}_1$ , is based on an air-to-ground (ATG) model [22] whose large-scale path loss depends on the elevation angle,  $\theta_{\text{el}}$ . The probability of a LoS connection is  $P_{\text{LoS}}(\theta_{\text{el}}) = (1 + a \exp(-b(\theta_{\text{el}} - a)))^{-1}$  where  $\theta_{\text{el}}$  is in degrees, and  $a$  and  $b$  are environmental parameters. The total path loss gain,  $\beta_1$ , combines LoS and non-line-of-sight (NLOS) components as

$$\beta_1 = \kappa_1 (P_{\text{LoS}}(\theta_{\text{el}}) + (1 - P_{\text{LoS}}(\theta_{\text{el}}))\eta_{\text{NLoS}}) d_1^{-\alpha_1}, \quad (2)$$

where  $\kappa_1 = 1$  is the reference path loss gain,  $\eta_{\text{NLoS}}$  is the NLOS attenuation,  $d_1 = \|\mathbf{q}_{\text{UAV}} - \mathbf{p}_{\text{BS}}\|_2$  is the BS-RIS distance, and  $\alpha_1$  is the path loss exponent. The small-scale fading is modeled as Rician, and the full channel matrix is a superposition of the deterministic LoS and stochastic NLOS components:

$$\mathbf{H}_1 = \beta_1^{1/2} \left( (K_1/(K_1 + 1))^{1/2} \mathbf{H}_{1,\text{LoS}} + (1/(K_1 + 1))^{1/2} \mathbf{H}_{1,\text{NLoS}} \right), \quad (3)$$

where  $K_1$  is the Rician K-factor for the BS-RIS link, and  $\mathbf{H}_{1,\text{NLoS}}$  consists of i.i.d.  $\mathcal{CN}(0, 1)$  random variables. Let the matrices  $\mathbf{P}_{\text{BS}} \in \mathbb{R}^{M \times 3}$  and  $\mathbf{P}_{\text{RIS}} \in \mathbb{R}^{N \times 3}$  contain the Cartesian coordinates of the BS antenna elements and RIS elements, respectively. The deterministic component,  $\mathbf{H}_{1,\text{LoS}}$ , is derived from the array geometry as the outer product of the array steering vectors:

$$\mathbf{H}_{1,\text{LoS}} = \mathbf{a}_{\text{RIS}}(\mathbf{P}_{\text{RIS}}, \mathbf{u}_{\text{AoA}}) \mathbf{a}_{\text{BS}}^H(\mathbf{P}_{\text{BS}}, \mathbf{u}_{\text{AoD}}), \quad (4)$$

where  $\mathbf{a}_{\text{RIS}}(\cdot) \in \mathbb{C}^{N \times 1}$  and  $\mathbf{a}_{\text{BS}}(\cdot) \in \mathbb{C}^{M \times 1}$ . The steering vector  $\mathbf{a}(\mathbf{P}, \mathbf{u}) \in \mathbb{C}^{L \times 1}$  for an array of  $L$  elements and a unit direction vector  $\mathbf{u} \in \mathbb{R}^{3 \times 1}$  is defined such that its  $l$ -th element is

$$[\mathbf{a}(\mathbf{P}, \mathbf{u})]_l = \exp \left( -j \frac{2\pi}{\lambda_c} \mathbf{p}_l^T \mathbf{u} \right), \quad (5)$$

where  $\mathbf{p}_l^T$  is the  $l$ -th row of  $\mathbf{P}$ . For the first hop, the unit direction vectors are  $\mathbf{u}_{\text{AoD}} = (\mathbf{q}_{\text{UAV}} - \mathbf{p}_{\text{BS}})/d_1$  and  $\mathbf{u}_{\text{AoA}} = -\mathbf{u}_{\text{AoD}}$ . The second hop channel,  $\mathbf{h}_{2,k} \in \mathbb{C}^{N \times 1}$ , models the link from the aerial RIS to ground user  $k$ . The large-scale path loss gain is defined as  $\beta_{2,k} = \kappa_2 d_{2,k}^{-\alpha_2}$ , where  $\kappa_2 > 0$  is the reference path loss gain and  $d_{2,k} = \|\mathbf{p}_k - \mathbf{q}_{\text{UAV}}\|_2$ . The small-scale fading is also Rician. Therefore, the RIS-user  $k$  channel can be given as

$$\mathbf{h}_{2,k} = \beta_{2,k}^{1/2} \left( (K_2/(K_2 + 1))^{1/2} \mathbf{h}_{2,k,\text{LoS}} + (1/(K_2 + 1))^{1/2} \mathbf{h}_{2,k,\text{NLoS}} \right), \quad (6)$$

where  $K_2$  is the Rician K-factor for the RIS-user link,  $\mathbf{h}_{2,k,\text{LoS}} \in \mathbb{C}^{N \times 1}$ , and  $\mathbf{h}_{2,k,\text{NLoS}} \in \mathbb{C}^{N \times 1}$  is a vector of i.i.d.  $\mathcal{CN}(0, 1)$  variables. The deterministic LoS component,  $\mathbf{h}_{2,k,\text{LoS}}$ , is the RIS array steering vector towards user  $k$ , given by  $\mathbf{a}_{\text{RIS}}(\mathbf{P}_{\text{RIS}}, \mathbf{u}_{\text{AoD},k})$ , where  $\mathbf{u}_{\text{AoD},k} = (\mathbf{p}_k - \mathbf{q}_{\text{UAV}})/d_{2,k}$ .

To formulate the system objective, we first define the aggregate second hop channel matrix as  $\mathbf{H}_2 = [\mathbf{h}_{2,1}, \dots, \mathbf{h}_{2,K}] \in \mathbb{C}^{N \times K}$ . The overall effective channel

from the BS to the users is then  $\mathbf{H}_{\text{eff}} = \mathbf{H}_2^H \Phi \mathbf{H}_1 \in \mathbb{C}^{K \times M}$ . The  $k$ -th row of this matrix, denoted  $\mathbf{h}_{\text{eff},k}^H$ , represents the end-to-end channel for user  $k$ . With the precoding matrix columns defined as  $\mathbf{G} = [\mathbf{g}_1, \dots, \mathbf{g}_K]$ , the signal-to-interference-plus-noise ratio (SINR) for user  $k$  is

$$\text{SINR}_k = \frac{|\mathbf{h}_{\text{eff},k}^H \mathbf{g}_k|^2}{\sum_{j=1, j \neq k}^K |\mathbf{h}_{\text{eff},k}^H \mathbf{g}_j|^2 + \sigma_n^2}. \quad (7)$$

### C. Uncertainty and Jitter Models

To capture the challenges of a practical deployment, we depart from the ideal assumption of perfect system knowledge and distinguish three cascaded channel representations. The estimated channel,  $\mathbf{H}^{\text{est}}$ , denotes the cascaded channel estimate available to the controller. In our formulation, it corresponds to a nominal, non-jittered channel and does not include an explicit CSI error term. The jittered channel,  $\tilde{\mathbf{H}}$ , is an intermediate, unobserved channel obtained by perturbing the nominal propagation geometry with UAV rotational jitter. The true physical channel,  $\mathbf{H}^{\text{true}}$ , is the channel used for throughput evaluation and is obtained by further corrupting the jittered channel with a cascaded CSI error. Thus, the controller observes  $\mathbf{H}^{\text{est}}$ , while the throughput is evaluated using  $\mathbf{H}^{\text{true}}$ . The first source of uncertainty, UAV jitter, is modeled as a rotational instability. We consider small angle deviations, allowing us to focus on phase alignment changes rather than gain pattern variations. Specifically,  $\delta_x, \delta_y, \delta_z \sim \mathcal{N}(0, \sigma_j^2)$  in radians around the roll, pitch, and yaw axes, respectively, with  $\sigma_j \leq 0.175$  rad (corresponding to  $10^\circ$ ). These induce a composite 3D rotation matrix  $\mathbf{R}_{\text{jitt}} = \mathbf{R}_{\text{yaw}}(\delta_z) \mathbf{R}_{\text{pitch}}(\delta_y) \mathbf{R}_{\text{roll}}(\delta_x)$ , where

$$\mathbf{R}_{\text{yaw}}(\delta_z) = \begin{bmatrix} \cos \delta_z & -\sin \delta_z & 0 \\ \sin \delta_z & \cos \delta_z & 0 \\ 0 & 0 & 1 \end{bmatrix}, \quad (8)$$

$$\mathbf{R}_{\text{pitch}}(\delta_y) = \begin{bmatrix} \cos \delta_y & 0 & \sin \delta_y \\ 0 & 1 & 0 \\ -\sin \delta_y & 0 & \cos \delta_y \end{bmatrix}, \quad (9)$$

$$\mathbf{R}_{\text{roll}}(\delta_x) = \begin{bmatrix} 1 & 0 & 0 \\ 0 & \cos \delta_x & -\sin \delta_x \\ 0 & \sin \delta_x & \cos \delta_x \end{bmatrix}. \quad (10)$$

This rotation perturbs the RIS element coordinates:

$$\tilde{\mathbf{P}}_{\text{RIS}} = \mathbf{P}_{\text{RIS}} \mathbf{R}_{\text{jitt}}^T. \quad (11)$$

The rotated coordinate matrix  $\tilde{\mathbf{P}}_{\text{RIS}}$  is then used to calculate the jittered LoS components,  $\tilde{\mathbf{H}}_{1,\text{LoS}}$  and  $\tilde{\mathbf{h}}_{2,k,\text{LoS}}$ . We form  $\tilde{\mathbf{H}}_1$  and  $\tilde{\mathbf{h}}_{2,k}$  by combining the jittered LoS components with the unchanged NLOS components. For user  $k$ , the jittered cascaded channel is defined as

$$\tilde{\mathbf{H}}_{\text{cascaded},k} \triangleq \text{diag}(\tilde{\mathbf{h}}_{2,k}^H) \tilde{\mathbf{H}}_1 \in \mathbb{C}^{N \times M}. \quad (12)$$

This represents the physical links under jitter while still assuming perfect CSI. The second source of uncertainty is imperfect CSI. We adopt a practical cascaded error model, in which the true physical channel  $\mathbf{H}_{\text{cascaded},k}^{\text{true}}$  is a noisy

version of the jittered channel  $\tilde{\mathbf{H}}_{\text{cascaded},k}$  and is modeled as

$$\mathbf{H}_{\text{cascaded},k}^{\text{true}} = \rho \tilde{\mathbf{H}}_{\text{cascaded},k} + \sqrt{1 - \rho^2} \mathbf{E}_k, \quad (13)$$

where  $\rho \in [0, 1]$  is the CSI quality parameter. The term  $\mathbf{E}_k \in \mathbb{C}^{N \times M}$  is a random error matrix with i.i.d. entries  $\mathcal{CN}(0, \sigma_k^2)$ , independent across users and of the jitter variables and small-scale fading, with variance  $\sigma_k^2 = \beta_1 \beta_{2,k}$ . This ensures the error power is appropriately scaled relative to the expected channel power for each user.

#### D. Problem Formulation

We formulate the problem of robust joint beamforming and RIS phase design. The objective is to design the BS beamforming matrix  $\mathbf{G}$  and the RIS phase shift matrix  $\Phi$  based only on the available channel estimates.

The instantaneous throughput is defined as

$$T \triangleq \sum_{k=1}^K \log_2 (1 + \text{SINR}_k^{\text{true}}), \quad (14)$$

where  $\text{SINR}_k^{\text{true}}$  denotes the SINR for user  $k$  computed using the true physical cascaded channel  $\mathbf{H}_{\text{cascaded},k}^{\text{true}}$ .

The optimization problem is then

$$\underset{\mathbf{G}, \Phi}{\text{maximize}} \quad \mathbb{E}[T] \quad (15a)$$

$$\text{s.t.} \quad \text{tr}(\mathbf{G}\mathbf{G}^H) \leq P_{\max}, \quad (15b)$$

$$|[\Phi]_{n,n}| = 1, \forall n. \quad (15c)$$

The expectation in (15a) is taken over all random quantities in the channel model, including user locations, small-scale fading, UAV jitter, and cascaded CSI errors. Constraint (15b) limits the BS transmit power to  $P_{\max}$ , and (15c) enforces strict unit-modulus coefficients on all RIS elements. Solving (15a) is challenging because the objective is nonconvex, the expectation does not admit a closed-form expression, and the unit-modulus constraint further complicates the feasible set.

## IV. PROPOSED DEEP REINFORCEMENT LEARNING FRAMEWORK

#### A. DRL Overview and Formulation

We adopt an actor-critic DRL architecture to handle the continuous actions in the joint beamforming and RIS phase design. The actor represents a deterministic policy that maps a state  $s$  to an action  $a$ . The critic learns the action value function  $Q(s, a)$  and is trained using the Bellman relation

$$Q(s, a) = r(s, a) + \gamma Q(s', a'), \quad (16)$$

where  $r(s, a)$  is the immediate reward,  $s'$  is the next state,  $a'$  is the next action, and  $\gamma \in [0, 1]$  is the discount factor.

The standard framework for modeling sequential decision-making problems in DRL is the MDP. A special case arises when an agent's actions do not influence future states, that is,  $\mathcal{P}(s'|s, a) = \mathcal{P}(s'|s)$ . This collapses the full MDP into a contextual bandit problem [23]. In this

paradigm, at each step, the agent observes a context and must choose an action to maximize the immediate reward, without needing to plan for future consequences. This bandit setting is formally enforced in the DRL framework by running one-step episodes and by setting the discount factor  $\gamma = 0$ . This reduces the Bellman equation to  $Q(s, a) = r(s, a)$ , compelling the agent to learn a myopic policy that is optimal for the current context only. Furthermore, specialized contextual bandit algorithms can be more sample-efficient than full DRL methods but often struggle to scale to problems with high-dimensional continuous action spaces.

#### B. DRL Algorithms

Our implementation is based on DDPG [24], and its successor, TD3 [25]. However, standard implementations of these algorithms, which typically use a tanh output layer, are insufficient for our problem constraints. Furthermore, in our contextual bandit setting, the immediate reward is  $y = r(s, a)$  with no bootstrap term, so we do not maintain separate target networks for the actor and critic.

We introduce a custom-constrained architecture where the actor network,  $\mu(\mathbf{s} | \theta^\mu)$ , outputs a raw, unconstrained vector. This vector is processed by a differentiable safety layer (DSL),  $\Pi(\cdot)$ , which implements a differentiable projection (safety layer) to enforce both the power constraint (15b) and the unit-modulus constraint (15c) [26]. The final policy is thus  $\pi(\mathbf{s}) = \Pi(\mu(\mathbf{s} | \theta^\mu))$ . Each critic is trained to minimize the mean squared error relative to the immediate reward,  $y = r$ . The loss for the critic is

$$L(\theta^Q) = \mathbb{E}_{(\mathbf{s}, \mathbf{a}, r) \sim \mathcal{D}} [(r - Q(\mathbf{s}, \mathbf{a} | \theta^Q))^2], \quad (17)$$

where  $\mathcal{D}$  is a replay buffer. Because the DSL is differentiable, gradients from the critic flow through the projection to the actor:

$$\nabla_{\theta^\mu} J \approx \mathbb{E}_{\mathbf{s} \sim \mathcal{D}} [\nabla_{\mathbf{a}} Q(\mathbf{s}, \mathbf{a} | \theta^Q) |_{\mathbf{a} = \pi(\mathbf{s})} \cdot \nabla_{\theta^\mu} \pi(\mathbf{s})]. \quad (18)$$

We add exploration noise to the raw actor output before projection so all exploratory actions remain feasible, where  $\mathcal{N} \sim \mathcal{N}(\mathbf{0}, \sigma^2 \mathbf{I})$ .

While DDPG provides a strong foundation, it can suffer from overestimated Q-values. To address this, we also implement TD3 [25]. TD3 introduces twin critics (via clipped double Q-learning) and delayed policy updates to stabilize training. In our contextual bandit formulation, the critic target simplifies to  $y = r$ , making the third TD3 mechanism (target policy smoothing) unused. We therefore only utilize the twin critic and delayed update components to improve stability over DDPG.

#### C. State Space

The state  $\mathbf{s} \in \mathcal{S}$  provides the agent with the contextual information for the current instance. It concatenates the geometric distances with the nominal channel estimates. This is defined as:

$$\mathbf{s} = (\{d_{2,k}\}_{k=1}^K, \Re\{\mathbf{H}_1^{\text{est}}\}, \Im\{\mathbf{H}_1^{\text{est}}\}, \Re\{\mathbf{H}_2^{\text{est}}\}, \Im\{\mathbf{H}_2^{\text{est}}\}), \quad (19)$$

---

**Algorithm 1** Constrained Contextual Bandit DDPG Algorithm

---

- 1: Initialize actor  $\mu(\mathbf{s} | \theta^\mu)$ , critic  $Q(\mathbf{s}, \mathbf{a} | \theta^Q)$ .
- 2: Initialize replay buffer  $\mathcal{D}$ .
- 3: **for** each context (one-step episode) **do**
- 4:   Environment resets: a new context
- 5:   Receive the full state  $\mathbf{s}$ .
- 6:   Select action with noise-before-projection:  $\mathbf{a} = \Pi(\mu(\mathbf{s} | \theta^\mu) + \mathcal{N})$ .
- 7:   Execute action  $\mathbf{a}$  and observe reward  $r$ .
- 8:   Store transition  $(\mathbf{s}, \mathbf{a}, r)$  in replay buffer  $\mathcal{D}$ .
- 9:   Sample minibatch of size  $B$ :  $\{(\mathbf{s}_j, \mathbf{a}_j, r_j)\}_{j=1}^B$  from  $\mathcal{D}$
- 10:   Set critic target:  $y_i = r_i$ .
- 11:   Update the critic by minimizing  $L(\theta^Q) = \frac{1}{B} \sum_i (y_i - Q(\mathbf{s}_i, \mathbf{a}_i | \theta^Q))^2$ .
- 12:   Update the actor using the policy gradient (18).
- 13: **end for**

---

where  $d_{2,k}$  is the distance between the RIS and user  $k$ ,  $\mathbf{H}_1^{\text{est}}$  is the estimated BS-RIS channel, and  $\mathbf{H}_2^{\text{est}} = [\mathbf{h}_{2,1}^{\text{est}}, \dots, \mathbf{h}_{2,K}^{\text{est}}]$  forms the estimated RIS-user channels. The agent observes non-jittered, error-free channels and must learn a mapping from this state to actions that perform well on average under the unobserved jitter and cascaded CSI errors.

#### D. Action Space

The action  $\mathbf{a} \in \mathcal{A}$  is a continuous vector of dimension  $2MK + 2N$  that encapsulates all the parameters the agent controls. This vector is defined as:

$$\mathbf{a} = [\text{vec}(\Re\{\mathbf{G}\}), \text{vec}(\Im\{\mathbf{G}\}), \Re\{\text{diag}(\boldsymbol{\Phi})\}, \Im\{\text{diag}(\boldsymbol{\Phi})\}]. \quad (20)$$

The first  $2MK$  entries of the action vector are reshaped into the complex BS beamforming matrix  $\mathbf{G} \in \mathbb{C}^{M \times K}$ , using half of the entries for the real part and half for the imaginary part. This raw beamforming matrix is then passed through the DSL, which enforces the transmit power constraint (15b) via a differentiable Frobenius-norm projection. In this way, the actor operates in an unconstrained Euclidean space, while the mapping to  $\mathbf{G}$  always respects the BS power budget.

The remaining  $2N$  entries of the action vector are reshaped as  $N$  two-dimensional real vectors, each corresponding to one RIS element. The DSL normalizes each of these vectors to unit norm and maps them to complex coefficients on the diagonal of  $\boldsymbol{\Phi}$ . This normalization enforces the strict unit-modulus constraint in (15c) for every RIS element, allowing the actor to output unconstrained values while ensuring that all executed actions are physically feasible.

#### E. Reward Function

The reward implements the objective in (15a) using the instantaneous throughput defined in (14). It is evaluated on the true cascaded channels, which include UAV

jitter and cascaded CSI errors, rather than on the nominal estimate observed by the agent. For a given action, the environment generates  $S$  independent realizations of jitter and CSI errors, constructs the corresponding true channels, and computes the throughput  $T^{(i)}$  for each realization as in (14). The reward is then defined as

$$r = \frac{1}{S} \sum_{i=1}^S T^{(i)}. \quad (21)$$

This Monte Carlo averaging reduces the variance of the reward signal due to the unobserved jitter and CSI errors, making learning more stable while remaining consistent with the optimization objective.

#### F. Training Dynamics

The training process follows the contextual bandit formulation, where each episode corresponds to an independent problem instance. At the beginning of an episode, a `reset` generates a new context. We sample a new set of  $K$  user locations from the predefined pool, recompute the corresponding large-scale and LoS components of the RIS-user links, and regenerate the NLOS components of the

MeBS-RIS and RIS-user channels from their respective complex Gaussian distributions. We keep the BS-RIS geometry and its large-scale and LoS terms fixed. This yields a statistically independent channel scenario for each episode. Within an episode, the agent performs a single `step` and the episode terminates, implementing the one-step contextual bandit structure described earlier. Furthermore, this sampling scheme exposes the agent to diverse channel realizations consistent with the average throughput objective.

## V. NUMERICAL RESULTS

In this section, we evaluate the performance of our proposed DRL framework. We construct a custom simulation environment in Python using PyTorch to model the downlink MISO system described in Section III. All DRL agents (both DDPG and TD3) are trained and evaluated on an NVIDIA GeForce RTX 3080. To ensure statistically significant and reproducible results, our evaluation methodology is aligned with the recommendations for rigorous DRL evaluation [27]. All DRL agents are averaged over 10 distinct random seeds. The classical optimizers, however, are deterministic, require no seed averaging, and are plotted without confidence intervals. For convenience, jitter standard deviations are reported in degrees in the figures. To validate our approach, we compare its performance against several key benchmark schemes. In the subsequent figures, these schemes are labeled as follows:

- AO-WMMSE: A conventional iterative algorithm based on the WMMSE criterion, adapted with AO to solve for the precoder and RIS phases separately [28].
- AO-WMMSE-SAA: A robust, non-DRL benchmark that uses SAA with the AO-WMMSE algorithm. It

optimizes under the same uncertainty distributions (jitter and imperfect CSI) as our DRL agent, serving as the primary traditional competitor for robust implementations [29].

- TD3 (BF-Only) and DDPG (BF-Only): An ablation study of our proposed model. Here, the DRL agent is trained to optimize only the BS beamforming matrix  $\mathbf{G}$ , while the RIS phase shifts  $\Phi$  are kept fixed to a random configuration. This baseline is used to quantify the performance gain achieved by actively optimizing the RIS.

The core idea of these experiments is to demonstrate the viability and robustness of our model-free DRL framework. We first establish the agents' convergence in an ideal environment. We then evaluate robustness to UAV jitter and imperfect CSI, considering these factors individually and jointly. Finally, we compare the computational complexity to highlight the practical deployment advantage of low online computational complexity.

#### A. Hyperparameters

The simulation environment models a realistic urban IoT scenario with a single BS ( $M = 4$ ), a UAV-mounted RIS ( $N = 16$ ), and  $K = 4$  users. The simulation, channel, and learning settings are summarized in Table II. Both the actor and critic are fully connected multilayer perceptrons (MLPs) with two hidden layers of 256 units each and ReLU activations. We denote their total numbers of trainable parameters by  $P_a$  and  $P_c$ , respectively.

#### B. Convergence Analysis

We first examine the convergence behavior of the DDPG and TD3 agents across four representative scenarios. Fig. 2(a) shows an ideal baseline with no jitter and perfect CSI ( $\sigma_j = 0.0^\circ$ ,  $\rho = 1.0$ ). Fig. 2(b) shows a jitter only case with UAV instability and perfect CSI ( $\sigma_j = 4.0^\circ$ ,  $\rho = 1.0$ ). Fig. 2(c) shows a CSI only case with imperfect estimation but a stable UAV ( $\sigma_j = 0.0^\circ$ ,  $\rho = 0.80$ ). Finally, Fig. 2(d) shows a joint uncertainty case with both jitter and CSI degradation ( $\sigma_j = 3.0^\circ$ ,  $\rho = 0.90$ ). For each scenario, both agents are trained using 10 independent training runs (random seeds) per algorithm. The x-axis shows training timesteps in thousands, the solid curves show the mean throughput (smoothed with a 2,000-step rolling window), and the shaded regions indicate 95% confidence intervals across seeds computed from the unsmoothed data, as shown in Fig. 2.

As illustrated in Fig. 2, both DDPG and TD3 successfully learn in all environments, converging from a low initial throughput to a high, stable performance. This confirms that the DRL approach remains viable even when trained in stochastic environments with multiple uncertainties. The TD3 algorithm, benefiting from its stability enhancements and twin critics that mitigate overestimation bias, consistently achieves a notably higher final throughput than DDPG, with the improvement typically becoming apparent at around  $10^5$  training steps for all cases. Under

Table II  
SIMULATION ENVIRONMENT AND LEARNING PARAMETERS

| Parameter                               | Value              |
|---|--------------------|
| <b>System Parameters</b>                |                    |
| BS antennas, $M$                        | 4                  |
| RIS elements, $N$                       | 16                 |
| Number of users, $K$                    | 4                  |
| Carrier frequency                       | 24 GHz             |
| BS position, $\mathbf{p}_{\text{BS}}$   | [0, 0, 20] m       |
| UAV position, $\mathbf{q}_{\text{UAV}}$ | [50, 0, 50] m      |
| Max BS power, $P_{\text{max}}$          | 1.0 W              |
| Noise power, $\sigma_n^2$               | -131 dBW           |
| <b>Channel Parameters</b>               |                    |
| ATG env. param., $a$                    | 9.61               |
| ATG env. param., $b$                    | 0.16               |
| Path-loss exp. (BS–RIS), $\alpha_1$     | 2.2                |
| NLoS attenuation, $\eta_{\text{NLoS}}$  | 0.5                |
| Path-loss const. (RIS–user), $\kappa_2$ | 0.001              |
| Path-loss exp. (RIS–user), $\alpha_2$   | 2.4                |
| K-factor (BS–RIS), $K_1$                | 3                  |
| K-factor (RIS–user), $K_2$              | 2                  |
| Monte Carlo samples, $S$                | 6                  |
| <b>DRL Agent Hyperparameters</b>        |                    |
| Learning rate                           | $1 \times 10^{-4}$ |
| Batch size, $B$                         | 32                 |
| Replay buffer size                      | 20,000             |
| Discount factor, $\gamma$               | 0.0                |
| Policy delay (TD3)                      | 3                  |
| Training steps, $T$                     | 200,000            |
| Evaluation episodes                     | 2,000              |
| RIS exploration noise (std.)            | 0.1                |
| Beamformer exploration noise (std.)     | 0.2                |
| <b>AO-Based Baseline Settings</b>       |                    |
| AO outer iterations, $a_{\text{max}}$   | 70                 |
| WMMSE inner iterations, $w_{\text{in}}$ | 12                 |
| Bisection steps, $n_{\text{bisect}}$    | 30                 |

ideal conditions, as shown in Fig. 2(a), the agents achieve a mean throughput of 11.08 bps/Hz for TD3 and 9.18 bps/Hz for DDPG in a separate 2,000-episode evaluation. Even under severe impairments, as in Fig. 2(b)–(d), the agents do not diverge but instead learn robust policies adapted to each uncertainty setting, with TD3 still outperforming DDPG. Furthermore, the shaded regions are very narrow, indicating low variability across seeds and convergence of all runs to similar values with similar trajectories. This confirms that the training procedure is stable.

#### C. Evaluation Analysis

We evaluate the final performance of the proposed DRL agents against the AO-WMMSE and robust AO-WMMSE-SAA baselines. We test under three types of uncertainty: UAV jitter with perfect CSI, imperfect CSI with no jitter, and joint jitter and CSI degradation. For each operating point (jitter level, CSI quality, or combined level), a separate agent is trained from scratch under the matched environment parameters. We train 10 such agents with different random seeds, and each trained agent is evaluated over 2,000 independent test episodes. Each point in the following plots represents the mean throughput over these evaluations, and the error bars indicate the 95% confidence intervals computed across the 10 seeds. For the

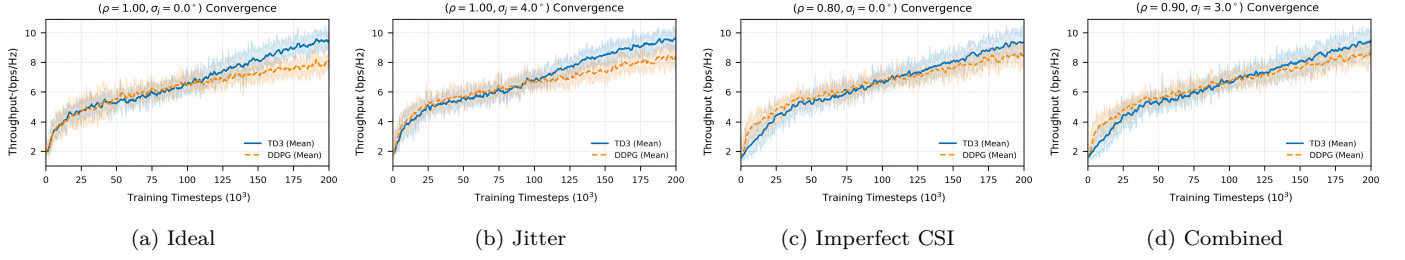


Fig. 2. Agent convergence for different scenarios.

joint-uncertainty scenario, we define five combined error levels L0–L4 as

$$\begin{cases} L0 : (\rho, \sigma_j) = (1.0, 0^\circ), & L1 : (0.9, 3^\circ), \\ L2 : (0.8, 5^\circ), & L3 : (0.6, 7^\circ), \\ L4 : (0.5, 10^\circ). & \end{cases} \quad (22)$$

Fig. 3(a) shows the impact of UAV jitter when CSI is perfect ( $\rho = 1.0$ ). The conventional AO-WMMSE benchmark degrades by approximately 35.4% as  $\sigma_j$  increases from  $0^\circ$  to  $10^\circ$ , indicating that a design optimized for a static geometry is highly sensitive to UAV jitter. In contrast, the DRL agents and the robust AO-WMMSE-SAA exhibit significantly milder degradation. The TD3 agent's throughput decreases by about 9.6%, while the AO-WMMSE-SAA drops by 13.8%. The DDPG agent shows the smallest relative loss, with only 5.6% degradation over the same jitter range.

Fig. 3(b) isolates the effect of CSI quality with a perfectly stable UAV ( $\sigma_j = 0.0^\circ$ ). Here, AO-WMMSE, which assumes perfect CSI, suffers a severe performance loss of about 59% as  $\rho$  decreases from 1.0 to 0.5. The robust AO-WMMSE-SAA and the DRL agents are substantially more tolerant to CSI errors. Across all  $\rho$  values, the TD3 agent remains within roughly  $\pm 7\%$  of the AO-WMMSE-SAA benchmark. The DDPG agent operates 13–22% below AO-WMMSE-SAA in absolute terms, but its relative degradation from  $\rho = 1.0$  to 0.5 is only 15.5%, comparable to the SAA benchmark's 19.1% drop.

Fig. 3(c) considers the combined uncertainty levels L0–L4 defined in (22). As both jitter and CSI errors increase, AO-WMMSE's performance collapses, with a total degradation of about 64.7% from L0 to L4. The robust AO-WMMSE-SAA degrades by 29.4%. The TD3 agent remains within approximately 0–12% of AO-WMMSE-SAA across all levels, while the DDPG agent exhibits the smallest relative loss at 22.6% but stays below SAA in absolute throughput. Together, these results confirm that the learned DRL policies maintain strong robustness under jitter-only, CSI-only, and combined uncertainty conditions.

The BF-only ablations across all three curves help separate the contributions of beamforming and RIS control to the overall performance. In the jitter robustness case, the mean throughput of TD3 and DDPG increase from 7.66 and 7.13 bps/Hz in the BF-only setting to 10.68 and 9.15 bps/Hz when the RIS is also optimized, corresponding to RIS-induced gains of approximately 3.02

and 2.02 bps/Hz (about 39% and 28% over their BF-only baselines). Under varying CSI quality, the gains are 3.15 versus 2.33 bps/Hz (about 45% versus 36%), and in the combined-uncertainty case they are 2.60 versus 2.03 bps/Hz (about 38% versus 31%). Across all scenarios, TD3's beamformer alone is only modestly better than DDPG's (by roughly 0.4–0.5 bps/Hz), whereas the larger share of the performance gap comes from the additional gain obtained when the RIS is controlled. This indicates that TD3 improves not only the active beamforming but also the joint exploitation of the RIS degrees of freedom.

#### D. Complexity Analysis

Each method incurs the same environment cost, since every simulator step evaluates a Monte Carlo robust throughput with  $S$  channel samples, requiring  $\mathcal{O}(SK^2NM)$  operations. On top of this, the DRL controllers differ only in their actor-critic update structure: DDPG performs one critic and one actor update per gradient step, leading to a training cost proportional to  $B(P_c + P_a)$ , i.e.,  $\mathcal{O}(B(P_c + P_a))$ , whereas TD3 maintains two critics and updates the actor once every  $\delta$  critic updates, with per-step cost proportional to  $B(2P_c + \frac{1}{\delta}P_a)$ , which remains of the same order  $\mathcal{O}(B(P_c + P_a))$  but with different constant factors. At test time, both DRL policies require a single actor forward pass plus the safety projection, yielding an inference complexity of  $\mathcal{O}(P_a)$  per decision. In contrast, the AO-WMMSE baseline solves a sequence of matrix-valued subproblems with per-solve complexity on the order of  $\mathcal{O}(a_{\max}(w_{\text{in}} n_{\text{bisect}} M^3 + N^3))$ , dominated by repeated  $M \times M$  linear solves and an  $N \times N$  eigendecomposition, while the robust AO-WMMSE-SAA variant preserves the same cubic scaling in  $M$  and  $N$  but adds a linear dependence on  $S_{\text{SAA}}$ , the number of SAA scenarios, through the scenario aggregation, yielding  $\mathcal{O}(a_{\max}(w_{\text{in}} n_{\text{bisect}} M^3 + S_{\text{SAA}} N^3))$ .

Table III reports the empirical offline and online runtimes for the considered methods under the parameter settings of Section V-A. In line with the above complexity discussion, the DRL agents incur a one-time offline training cost but achieve sub-millisecond inference, since deployment reduces to a single actor forward pass with the safety projection. In contrast, AO-WMMSE and AO-WMMSE-SAA require no training but take several hundred milliseconds per decision, which makes them impractical for fast time-varying UAV scenarios. In the proposed

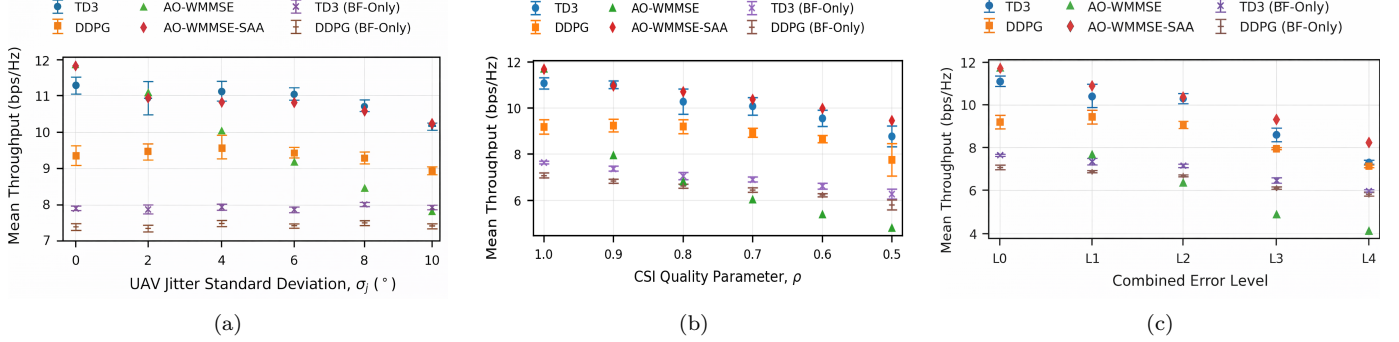


Fig. 3. Evaluation figures: (a) Performance vs. UAV jitter ( $\rho = 1.0$ ), (b) Performance vs. CSI quality ( $\sigma_j = 0.0^\circ$ ), and (c) Performance vs. combined error level.

contextual bandit formulation, we omit target networks which lowers both memory usage and per-update overhead compared to standard DDPG and TD3 implementations and contributes to the higher training throughput observed in Table III. Although TD3 maintains twin critics, its delayed actor updates partly offset the additional critic cost, and in our implementation it achieves slightly higher effective steps per second than DDPG.

Table III  
COMPUTATIONAL COMPLEXITY COMPARISON

| Algorithm    | Offline Training Time (s) | Steps/s | Online Inference Time (ms) |
|--------------|---------------------------|---------|----------------------------|
| TD3          | 1227.2                    | 162.97  | 0.62                       |
| DDPG         | 1336.6                    | 149.63  | 0.62                       |
| AO-WMMSE     | 0.00                      | 0.00    | 370.5                      |
| AO-WMMSE-SAA | 0.00                      | 0.00    | 551.01                     |

## VI. CONCLUSION

This paper proposed a constrained, model-free DRL framework for joint BS beamforming and RIS phase control in the presence of UAV attitude jitter and imperfect cascaded CSI. By formulating each channel realization as a contextual bandit and embedding a differentiable feasibility projection, the framework enables stable end-to-end learning while guaranteeing transmit power and unit-modulus constraints. We addressed uncertainty at training time by aligning the reward with the expected throughput objective. Also, we developed a DDPG agent to achieve the objective, and a TD3 agent to improve stability. Comprehensive experiments show that the learned agents perform competitively in both ideal and uncertain regimes, maintaining strong throughput relative to iterative AO/WMMSE baselines while reducing online decision latency to the sub-millisecond scale. Future research directions include addressing stricter quality of service (QoS) constraints, incorporating a phase-dependent amplitude RIS model for more realistic implementation, extending to scenarios with multiple UAVs for increased coverage, and scaling to a larger set of RIS elements while maintaining proper hyperparameter tuning that preserves stability.

## ACKNOWLEDGMENT

We acknowledge the support provided by King Fahd University of Petroleum and Minerals (KFUPM), Dhahran 31261, Saudi Arabia, through the Interdisciplinary Research Center for Communication Systems and Sensing (IRC-CSS).

## REFERENCES

- [1] Z. Wei, H. Qu, Y. Wang, X. Yuan, H. Wu, Y. Du, K. Han, N. Zhang, and Z. Feng, "Integrated sensing and communication signals toward 5G-A and 6G: A survey," *IEEE Internet Things J.*, vol. 10, no. 13, pp. 11 068–11 092, 2023.
- [2] K. David and H. Berndt, "6G vision and requirements: Is there any need for beyond 5G?" *IEEE Veh. Technol. Mag.*, vol. 13, no. 3, pp. 72–80, 2018.
- [3] M. M. Salim, S. I. Al-Dharrab, D. B. Da Costa, and A. H. Muqaibel, "Cooperative NOMA meets emerging technologies: A survey for next-generation wireless networks," *IEEE Open J. Commun. Soc.*, vol. 6, pp. 9247–9286, 2025.
- [4] E. Björnson, H. Wymeersch, B. Mattheisen, P. Popovski, L. Sanguinetti, and E. de Carvalho, "Reconfigurable intelligent surfaces: A signal processing perspective with wireless applications," *IEEE Signal Process. Mag.*, vol. 39, no. 2, pp. 135–158, 2022.
- [5] N. Cheng, S. Wu, X. Wang, Z. Yin, C. Li, W. Chen, and F. Chen, "AI for UAV-assisted IoT applications: A comprehensive review," *IEEE Internet Things J.*, vol. 10, no. 16, pp. 14 438–14 461, 2023.
- [6] W. Yuan, C. Liu, F. Liu, S. Li, and D. W. K. Ng, "Learning-based predictive beamforming for UAV communications with jittering," *IEEE Wirel. Commun. Lett.*, vol. 9, no. 11, pp. 1970–1974, 2020.
- [7] B. Zheng, C. You, W. Mei, and R. Zhang, "A survey on channel estimation and practical passive beamforming design for intelligent reflecting surface aided wireless communications," *IEEE Commun. Surveys Tuts.*, vol. 24, no. 2, pp. 1035–1071, 2022.
- [8] B. Shamasundar, N. Daryanavardan, and A. Nosratinia, "Channel training & estimation for reconfigurable intelligent surfaces: Exposition of principles, approaches, and open problems," *IEEE Access*, vol. 11, pp. 6717–6734, 2023.
- [9] Q. Wu, S. Zhang, B. Zheng, C. You, and R. Zhang, "Intelligent reflecting surface aided wireless communications: A tutorial," *IEEE Trans. Commun.*, vol. 69, no. 5, pp. 3313–3351, 2021.
- [10] H. Zhou, M. Erol-Kantarci, Y. Liu, and H. V. Poor, "A survey on model-based, heuristic, and machine learning optimization approaches in RIS-aided wireless networks," *IEEE Commun. Surveys Tuts.*, vol. 26, no. 2, pp. 781–823, 2024.
- [11] C. Huang, R. Mo, and C. Yuen, "Reconfigurable intelligent surface assisted multiuser MISO systems exploiting deep reinforcement learning," *IEEE J. Sel. Areas Commun.*, vol. 38, no. 8, pp. 1839–1850, 2020.
- [12] K. Stylianopoulos, G. Alexandropoulos, C. Huang, C. Yuen, M. Bennis, and M. Debbah, "Deep contextual bandits for orchestrating multi-user MISO systems with multiple RISs," in *Proc. IEEE Int. Conf. Commun. (ICC)*, 2022, pp. 1556–1561.

- [13] D. Pereira-Ruisánchez, Ó. Fresnedo, D. Pérez-Adán, and L. Castedo, “Deep contextual bandit and reinforcement learning for IRS-assisted MU-MIMO systems,” *IEEE Trans. Veh. Technol.*, vol. 72, no. 7, pp. 9099–9114, 2023.
- [14] H. Zhang, M. Huang, H. Zhou, X. Wang, N. Wang, and K. Long, “Capacity maximization in RIS-UAV networks: A DDQN-based trajectory and phase shift optimization approach,” *IEEE Trans. Wireless Commun.*, vol. 22, no. 4, pp. 2583–2591, 2023.
- [15] D. Wang, J. Li, Q. Lv, Y. He, L. Li, Q. Hua, O. Alfarraj, and J. Zhang, “Integrating reconfigurable intelligent surface and AAV for enhanced secure transmissions in IoT-enabled RSMA networks,” *IEEE Internet Things J.*, vol. 12, no. 8, pp. 9405–9419, 2025.
- [16] A. A. Puspitasari and B. M. Lee, “TD3 algorithm-based SWIPT with UAV-RIS assistance for MIMO communication,” *IEEE Trans. Veh. Technol.*, vol. 74, no. 4, pp. 6284–6293, 2025.
- [17] S. Hong, C. Pan, H. Ren, K. Wang, K. K. Chai, and A. Nallanathan, “Robust transmission design for intelligent reflecting surface-aided secure communication systems with imperfect cascaded CSI,” *IEEE Trans. Wireless Commun.*, vol. 20, no. 4, pp. 2487–2501, 2021.
- [18] M. M. Salim, K. M. Rabie, and A. H. Muqaibel, “Robust energy-efficient DRL-based optimization in UAV-mounted RIS systems with jitter,” *IEEE Commun. Lett.*, 2025, early access.
- [19] B. Saglam, D. Gurgunoglu, and S. S. Kozat, “Deep reinforcement learning based joint downlink beamforming and RIS configuration in RIS-aided MU-MISO systems under hardware impairments and imperfect CSI,” in *Proc. IEEE Int. Conf. Commun. Workshops*. IEEE, 2023, pp. 66–72.
- [20] A. B. Adam, X. Wan, M. A. Elhassan, M. S. A. Muthanna, A. Muthanna, N. Kumar, and M. Guizani, “Intelligent and robust UAV-aided multiuser RIS communication technique with jittering UAV and imperfect hardware constraints,” *IEEE Trans. Veh. Technol.*, vol. 72, no. 8, pp. 10 737–10 753, 2023.
- [21] A. Bansal, N. Agrawal, K. Singh, C.-P. Li, and S. Mumtaz, “RIS selection scheme for UAV-based multi-RIS-aided multiuser downlink network with imperfect and outdated CSI,” *IEEE Trans. Commun.*, vol. 71, no. 8, pp. 4650–4664, 2023.
- [22] A. Al-Hourani, S. Kandeepan, and S. Lardner, “Optimal lap altitude for maximum coverage,” *IEEE Wirel. Commun. Lett.*, vol. 3, no. 6, pp. 569–572, 2014.
- [23] T. Lattimore and C. Szepesvári, *Bandit Algorithms*. Cambridge, UK: Cambridge University Press, 2020.
- [24] T. P. Lillicrap, J. J. Hunt, A. Pritzel, N. Heess, T. Erez, Y. Tassa, D. Silver, and D. Wierstra, “Continuous control with deep reinforcement learning,” *arXiv preprint arXiv:1509.02971*, 2015.
- [25] S. Fujimoto, H. Hoof, and D. Meger, “Addressing function approximation error in actor-critic methods,” in *Proc. Int. Conf. Mach. Learn. (ICML)*. PMLR, 2018, pp. 1587–1596.
- [26] G. Dalal, K. Dvijotham, M. Vecerik, T. Hester, C. Paduraru, and Y. Tassa, “Safe exploration in continuous action spaces,” *arXiv preprint arXiv:1801.08757*, 2018, accessed: Dec. 2025. [Online]. Available: <https://arxiv.org/abs/1801.08757>
- [27] P. Henderson, R. Islam, P. Bachman, J. Pineau, D. Precup, and D. Meger, “Deep reinforcement learning that matters,” in *Proc. AAAI Conf. Artif. Intell.*, vol. 32, no. 1, 2018.
- [28] Q. Shi, M. Razaviyayn, Z.-Q. Luo, and C. He, “An iteratively weighted MMSE approach to distributed sum-utility maximization for a MIMO interfering broadcast channel,” *IEEE Trans. Signal Process.*, vol. 59, no. 9, pp. 4331–4340, 2011.
- [29] S. Kim, R. Pasupathy, and S. G. Henderson, “A guide to sample-average approximation,” Cornell University, Tech. Rep., 2011. [Online]. Available: <https://people.orie.cornell.edu/shane/pubs/SAAGuide.pdf>